# Orienting Tetracene and Pentacene Thin Films onto Friction-Transferred Poly(tetrafluoroethylene) Substrate

**Martin Brinkmann,* Sabine Graff, Christine Straupé, and Jean-Claude Wittmann**

*Institut Charles Sadron, 6 rue Boussingault, 67083 Strasbourg, France*

**Christian Chaumont**

*Ecole de Chimie, Polymères et Matériaux de Strasbourg, 23 rue du Loess, 67000 Strasbourg, France*

**Frank Nuesch, Anver Aziz, Michel Schaer, and Libero Zuppiroli**

*Ecole Polytechnique Fédérale de Lausanne, 1015 Lausanne, Switzerland*

*Received: February 18, 2003; In Final Form: May 22, 2003*

Oriented films of tetracene and pentacene have been obtained by high vacuum sublimation onto oriented poly(tetrafluoroethylene) (PTFE) substrates. Polymorphism, orientation, and morphology of the pentacene and tetracene films are studied as a function of deposition parameters [substrate temperature ($T_s$), deposition time ($t$), and deposition rate ($\tau$)] using X-ray and electron diffraction, transmission and scanning electron microscopies and atomic force microscopy (AFM). Oriented films of the triclinic structures reported by Campbell et al. (*Acta Crystallogr.* **1961**, *14*, 705; **1962**, *15*, 289) have been obtained in well-defined $T_s$-ranges. Oriented acene films of 50 nm consist of a continuous texture of flat-lying and terraced domains with a dense (0 0 1) contact plane and a high degree of in-plane orientation. Specific nucleation sites of pentacene on the PTFE substrate have been identified by AFM in the early stage of deposition. The similarity found in the growth phenomenology of tetracene and pentacene allows for identification of the mechanism responsible for oriented growth which involves (i) ledge-directed nucleation and (ii) confined growth of nanocrystals by the PTFE meso-scale relief, e.g. nanoscopic grooves between successive PTFE fibrils. In addition, various crystal defects, e.g. edge dislocations, have been identified by high-resolution TEM.

## I. Introduction

In the past decades, electroactive organic molecules have attracted much attention owing to their versatility and unique electronic properties of interest for the design of optoelectronic and electronic devices including organic light-emitting diodes (OLEDs) and organic field effect transistors (OFETs).[2] Both tetracene (TEN) and pentacene (PEN) have recently emerged as promising molecular systems to design OFETs with charge carrier mobilities as large as 0.5−0.7 $cm^2/V$ s and on/off ratio of $10^8$, similar to hydrogenated amorphous silicon.[3−5] When deposited onto doped silicon wafers plus insulating $SiO_2$, acenes (ACN) form large terraced and dendritic domains of a few tens of microns in a regime of diffusion-limited aggregation.[6,7] Both grain boundaries and intrinsic polymorphism of PEN have been shown to play a key role in the limitation of the field effect mobility.[2,3,8] The control of the structure, the orientation, and the overall morphology in sublimed thin films appears accordingly as a key factor for the improvement of transport properties in ACN thin films.

At least three different polymorphs of pentacene have been identified so far, which are characterized by $d_{001}$ values of 1.41, 1.45, and 1.55 nm.[3,9,10] Pentacene platelets are obtained by crystallization in 1,3,5-trichlorobenzene or growth from the vapor phase.[9,10] The first crystal structure of the platelets (hereafter $\beta$-PEN), which is characterized by $d_{001}$=1.45 nm, was proposed by Campbell et al.:[1] space group $P$-1, $a$ = 0.606 nm, $b$ = 0.790 nm, $c$ = 1.488 nm, $\alpha$ = 96.74°, $\beta$ = 100.54°, $\gamma$ = 94.2°, and $Z$ = 2. Recent works have identified a different structure of platelets (hereafter $\gamma$-PEN)[9,10] with the following reduced unit cell parameters at 293 K: $P$-1, $a$ = 0.628 nm; $b$ = 0.771 nm; $c$ = 1.44 nm, $\alpha$ = 76.75°; $\beta$ = 88.01°, and $\gamma$ = 84.52°. In addition to these bulk structures, pentacene is found to crystallize in a so-called "thin film phase" (hereafter $\alpha$-PEN), which is characterized by a $d_{001}$ spacing of 1.55 nm.[2,9] In thin films, the observed crystal structure has been found to depend on both substrate temperature ($T_s$) and film thickness ($h$).[11] In pentacene films deposited onto $SiO_2$, for instance, the crystal structure progressively changes from $\alpha$ to $\beta$ with increasing film thickness.[11]

In-plane orientation of pentacene films has been performed in order to improve the transport properties in OFETs using rubbed pentacene layers[12] or rubbed poly(vinyl alcohol) films[13] as orienting substrates. However, the intimate growth mechanism responsible for orientation of pentacene on these substrates has not been identified so far. Alternatively, thin PTFE films obtained by friction transfer can be used as orienting media onto various smooth substrates such as silicon and ITO glass, for instance.[14] Merits of oriented PTFE films are their remarkable nucleating and orienting properties, chemical and thermal stability, and optical transparency (visible range). By today, PTFE films have been successfully used for the orientation of a large variety of small molecules including sexithiophene (T6),[15] paraphenylene-vinylene oligomers,[16] diacetylenes,[17] tris-(8-hydroxyquinoline)aluminum(III) ($Alq_3$),[18] phthalocyanines

* Corresponding author. e-mail: brinkman@ics.u-strasbg.fr.

10.1021/jp030217q CCC: $25.00 
Published on Web 08/28/2003

(CuPc and TiOPc),[19] and various organic dyes.[20] Concerning the origin of oriented growth, different mechanisms have been invoked, including 1D epitaxy, 2D epitaxy, and graphoepitaxy.[19,21] Recent studies have demonstrated that the mesoscale structure of the PTFE films, e.g. the existence of macrosteps (ledges), and the molecular-scale structure of the PTFE chains are playing complementary roles in the orientation mechanism of organic conjugated molecules.[18,19] For instance, no oriented growth is observed onto irradiated PTFE areas where cross-linking of the PTFE chains has occurred, underlining the importance of the molecular-scale order of the PTFE chains.[18] In addition, AFM analysis of the film morphology in the very beginning of TiOPc film growth by vacuum deposition has evidenced that PTFE ledges (macrosteps) play a key role in the heterogeneous nucleation of nanocrystallites.[19]

The present study is dedicated to the mechanism of growth in oriented pentacene thin films deposited onto oriented PTFE. We have investigated the effect of several deposition parameters, e.g. $T_s$ and $h$, on the morphology and structure of the pentacene thin films. We demonstrate that the orientation degree of pentacene films depends on both deposition parameters and the mesoscale relief of the PTFE substrates. The paper is organized in the following manner: section II summarizes the experimental conditions and section III presents experimental results concerning the morphology, the structure, and the optical properties. In section IV, we discuss the mechanism for oriented growth of pentacene onto PTFE.

## II. Experimental Section

ACN thin films were grown by high vacuum sublimation using an Edwards Auto306 evaporator system from fused quartz crucibles heated by a tungsten filament. The base pressure of the evaporation chamber was $10^{-7}$ mbar for PEN and $10^{-6}$ mbar for TEN. The film thickness and the deposition rate ($\tau$) (0.2−6.0 nm/min) were controlled by using a quartz microbalance placed in the vicinity of the substrate holder. TEN and PEN starting material (Aldrich, 98%) were purified by gradient sublimation. The substrate temperature in the range −25 to 100 °C was measured at the film surface with a Pt 100 resistance fixed on the substrate surface using silver paste. Re-evaporation of pentacene and tetracene has been observed for substrate temperatures above 100 and 40 °C, respectively. After deposition, samples were rapidly quenched to room temperature (cooling rate, 0.5−1.0 °C/s) by using a liquid nitrogen cooling system in order to prevent modification of the film morphology, e.g. by annealing.

PTFE films were prepared according to the method described elsewhere[14,18] by sliding a PTFE rod at a constant pressure (5 bar) against a glass slide (Corning 2947) held at 250−300 °C. Prior to PTFE deposition, the glass substrates were cleaned by an appropriate method used for ITO.[22] The cleaning of glass substrates involves successively: (i) ultrasonication in acetone and ethanol, (ii) soft mechanical scrubbing with a soft nylon brush (commercially available tooth brush), and (iii) thorough rinsing in ultrapure Milli-Q water. The purpose of this cleaning procedure, especially the mechanical scrubbing, is to remove microparticles that could perturb the friction-transfer of PTFE. It is found that both the degree of coverage of glass by PTFE and the uniformity (roughness) of the PTFE films are intimately related to the quality of the cleaning of the glass substrate.

The film orientation was first investigated by polarized optical microscopy using a LEICA DM-RX microscope. For the TEM study, films of thickness 5−50 nm were coated with a carbon film, floated off on water, and then transferred onto copper microscope grids. The films were studied in bright field and diffraction modes with a 120 kV Philips CM12 electron microscope. Tapping mode AFM was performed on a Nanoscope III using $Si_3N_4$ cantilevers oscillating at a frequency in the range 250−300 kHz. X-ray diffraction was performed on a Siemens D5000 diffractometer in ($\theta$, $2\theta$) mode using Cu K$\alpha$ radiation ($\lambda = 1.54$ Å). UV−vis−near-IR absorption of the thin films (300−900 nm) was measured on a Shimadzu UV-2101PC spectrometer with polarized incident light and spectral resolution of 1 nm. The film orientation with respect to the incident light was controlled by mean of a goniometer: parallel orientation is obtained when the incident beam polarization is parallel to the PTFE sliding direction ($c_{PTFE}$ axis). The crystal structure and diffraction patterns were generated with the appropriate modules of the Cerius[2] program (Acelrys, Waltham, MA and Cambridge, UK). It has to be stressed that the unit cell parameters of TEN and $\beta$-PEN used in this study for the indexation/simulation of the SAED patterns are those of the reduced cells given in the Introduction.

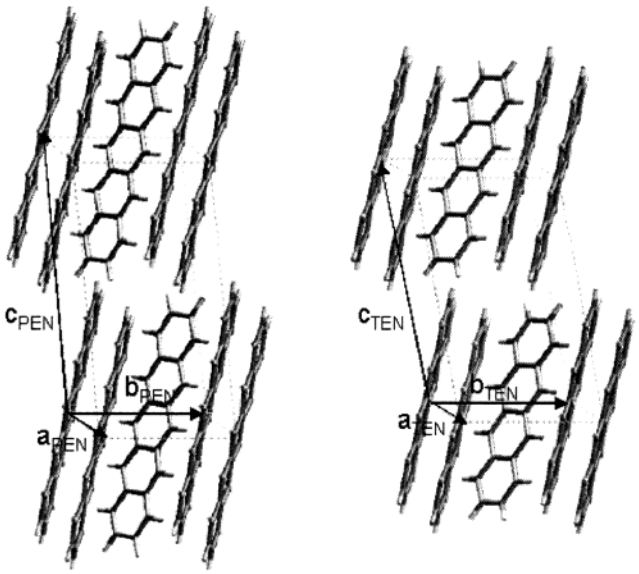


**Figure 1.** Reduced unit cells of the triclinic structures of TEN and PEN as determined by Campbell et al.[1]

## III. Results

**III.1. Morphology.** *(a) Early Stage of Deposition: Nucleation and Growth.* Several reports have pointed to the role of PTFE macrosteps (ledges) in the nucleation of organic molecules deposited on ultraoriented PTFE substrate.[18,19] To establish the role of PTFE ledges in the nucleation of PEN domains, we have grown thin films of 1 and 5 nm (surface coverage below 10%) at $T_s = 90$ °C. The typical surface topography probed by AFM is depicted in Figure 2.

From the point of view of morphology, the following characteristic features are observed in friction-transferred PTFE films (see Figure 2 and Table 1): (i) extended and flat PTFE stripes (RMS roughness below 2 nm) with a typical width >200 nm, (ii) very narrow PTFE nanofibrils (typical width below 30 nm), (iii) nanoscopic grooves with a mean height of 30 nm and width of ca. 10−50 nm, and (iv) transverse nanofibrils linking successive PTFE stripes.

The morphology in the pentacene films of 1 nm shown in Figure 2 reveals several interesting features that allow us to draw a scenario for the nucleation of pentacene on this substrate. Hemispherically shaped pentacene aggregates, a few tens of nanometers in diameter, are observed to be preferentially

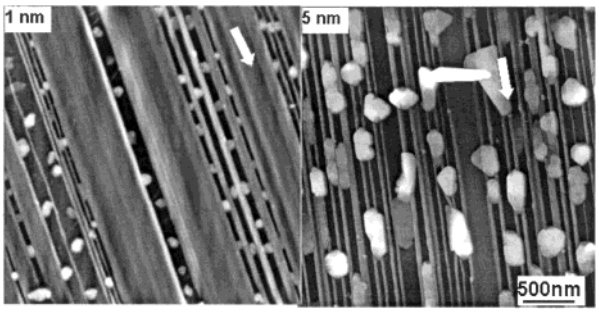


**Figure 2.** Early stage of growth in pentacene thin films deposited onto oriented PTFE probed by AFM. The PEN films are grown at $T_s$ = 90 °C and $\tau$ = 3.0 nm/min. The white arrows indicate the PTFE chain axis direction.

nucleated along PTFE nanofibrils and confined in the grooves between successive fibrils. In some grooves, nuclei are found to be regularly spaced at a periodicity of ca. 200−400 nm. This situation is very similar to that encountered in 5 nm-thick amorphous $Alq_3$ films grown at $T_s$ = 25 °C that show parallel rows of nanodroplets.[18] In contrast to this, large PTFE stripes are found to be almost exempt from pentacene nuclei. Using phase-mode imaging on these PTFE areas, we did not observe any contrast that would hint at the presence of a continuous pentacene monolayer. As the thickness of the film increases to 5 nm (see Figure 2), we observe the formation of terraced domains with a high in-plane aspect ratio, typically >10, which are also confined between PTFE ledges. Apparently, these domains have been enforced to grow parallely to the ledge direction due to the confinement by the PTFE nanofibrils. Only when the height of these domains exceeds that of the ledge is the lateral growth of the domains possible. As the film thickness increases from 1 to 5 nm, we observe how the hemispherically shaped pentacene aggregates transform into microcrystallites with sharper edges and a terraced structure. Similarly to TiOPc, there is very likely an increase of crystalline order within the domains with increasing film thickness.[19]

*(b) Effect of Substrate Temperature.* The typical morphologies of 50-nm-thick ACN films are depicted in Figure 3. Table 1 collects the main structural and morphological characteristics of the PEN thin films.

Oriented TEN and PEN films (50 nm) grown at $T_s$ = 25 and 90 °C, respectively, consist of a continuous texture of flat-lying and terraced domains oriented with their long axis parallel to $c_{PTFE}$. Given the similarity of the growth habit for TEN and PEN, we will essentially focus on the case of PEN thin films in the following.

The sequences of parts a−c and d−f of Figure 4 depict the surface morphology in oriented PEN films onto PTFE obtained at different $T_s$ (28−90 °C) probed by AFM and TEM, respectively. The main effect of increasing $T_s$ is an increase of the mean microcrystallite size between 50 and 100 nm for $T_s$ = 28 °C and about 1−3 $\mu$m for $T_s$ = 90 °C. Conversely, the density of domains per unit surface is found to decrease with increasing $T_s$.

The films grown at room temperature exhibit two type of domains (see Figure 4a): (i) small hemispherically shaped domains of mean size 50−100 nm and (ii) elongated domains in the $c_{PTFE}$ direction (mean size 300−600 nm). The latter domains show a terraced structure clearly visible in phase contrast. The height of the terraces measured by AFM from a batch of 10−15 samples is 1.3 ± 0.3 nm. Within experimental errors, this value is close to the interplanar spacing $d_{001}$ = 1.55 nm obtained by XRD. In contrast to the films grown onto Si-(100), no extended dendritic domains are formed on PTFE, since the lateral extension of the dendrites is hindered by the mesoscale relief (ledges) of the PTFE.

For $T_s$ = 50 °C, among a majority of flat-lying domains, we observe a small fraction of standing lamellar crystallites (see Figure 4b) that appear as dark stripes in the TEM micrograph of Figure 4e. These lamellae are oriented in such a way that their plane is perpendicular to both the plane of the substrate and the PTFE chain direction. The mean height of these domains determined by AFM is approximately 300 nm. The proportion of these standing crystallites depends strongly on the deposition rate: slow deposition rates (below 1 nm/min) favor larger proportions of standing crystals. As a matter of fact, further increasing $T_s$ above 70 °C prevents the formation of standing domains. For $T_s \geq$ 70 °C, a polycrystalline texture is observed, most crystallites showing sharp edges with well-defined angles in addition to a terraced structure. Temperatures above 90 °C for PEN and 35 °C for TEN result in total re-evaporation of the films. PEN films have, however, been obtained for $T_s$ up to 120 °C onto $SiO_2$ for higher deposition rates.[11] The difference in the temperature at which re-evaporation occurs is attributed to different sticking coefficients of ACNs on PTFE and $SiO_2$, likely traducing a smaller molecule−substrate interaction in the case of PTFE substrate.

*(c) Crystal Defects.* Structural defects, e.g. edge and screw dislocations, are believed to affect both transport properties in OFETs and optical properties, since they can act as traps for both charge carriers and excitons, respectively. However, microscopic evidence for such defects has only been gained for powdered samples of pentacene.[23]

In Figure 4f, a significant proportion of microcrystallites show typical Bragg fringes. Such fringes are commonly observed when, for instance, a lamellar crystal is slightly bent or subjected to stress.[24] Bragg fringes are mainly encountered in the vicinity of grain boundaries between crystals with different azimuthal orientations. In addition, Moiré patterns are observed to superpose to Bragg fringes in some cases (not shown). These observations are indicative of the presence of disorder, both at the mesoscale (misorientation of microcrystallites) and at the molecular scale within the microcrystals. It is however not possible to ascertain that all defects were present in the films prior to the removal of the PTFE/ACN bilayer from the glass substrate.

In Figure 5, we have depicted HRTEM micrographs showing typical stacking defects observed in edge-on PEN nanocrystallites (films grown at $T_s$ = 50 °C). Edge-on domains reveal a succession of dark and light stripes with a total periodicity of 1.52 ± 0.05 nm. This spacing is close to the value of $d_{001}$ reported for α-PEN, i.e., the distance between successive PEN molecular planes. Accordingly, dark stripes are attributed to the section of $(001)_\alpha$ molecular planes in a direction perpendicular to the plane. As seen in Figure 5a,c, typical edge dislocations are found in standing α-PEN nanocrystals. The most probable Burger's vector corresponds to $c_{PEN}$ in the reduced unit cell. Figure 5b depicts another typical defect where the growth direction of the crystallite has been locally perturbed, which could be due to a misorientation of the underlying PTFE substrate. The central part of the nanocrystal is oriented at 12.5° from the rest of the domain. This situation results in the presence of two edge dislocations close to the lateral facets of the nanocrystal.

**III.2. Impact of Substrate Temperature on Crystal Structure and Orientation.** In this section, we will analyze successively, three major points. First, we will discuss the occurrence

**TABLE 1: TEM and X-Ray Characteristics of 50 nm Thick PEN Films Deposited onto Oriented PTFE Substrate as a Function of Increasing Substrate Temperature ($T_s$)**

| substrate temp ($T_s$) | morphology (AFM, SEM) | ED pattern | X-ray diffraction |
|---|---|---|---|
| 25 °C | hemispherical domains (100-500 nm in size) elongated domains along $c_{PTFE}$ (300-600 nm in size) | continuous diffraction rings of α-PEN characteristic $d_{hkl}$ values: 0.473, 0.385, 0.298, and 0.234 nm | $(00n)_\alpha$ reflections ($1 \le n \le 4$ ) at 1.57, 0.78, 0.521, and 0.388 nm |
| 50−75 °C | flat-lying domains with (001) contact plane (mean size < 1 $\mu$m) standing α-PEN lamellar-shaped crystallites | coexistence of continuous diffraction rings (unoriented PEN crystals) and sharp reflections (oriented $\beta$-PEN) | coexistence of α and $\beta$ forms increasing intensity of $(00n)_\beta$ reflections decreasing intensity of $(00n)_\alpha$ reflections |
| 75−90 °C | elongated microcrystals along $c_{PTFE}$ (mean length: 1−3 $\mu$m) Bragg fringes at domain boundaries | uniform oriented $\beta$-PEN films with $a_{PEN}//c_{PTFE}$ sharp reflections with negligible arcing zone axes: [112] and [012] | $(00n)_\beta$ reflections ($1 \le n \le 4$ ) at 1.46 and 0.73 nm |

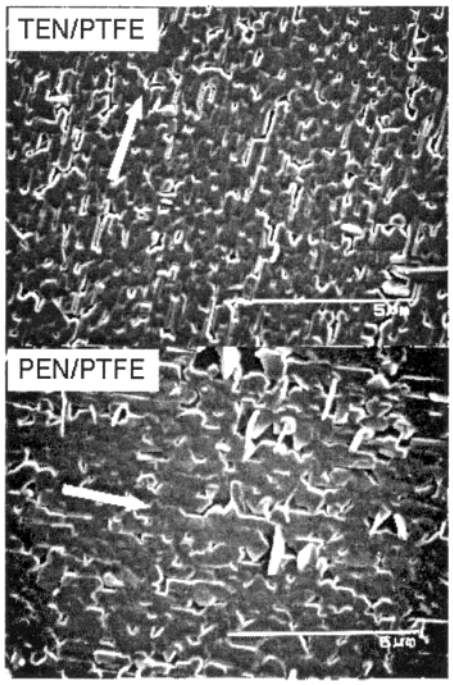


**Figure 3.** Comparison of the morphology oriented TEN (A) and $\beta$-PEN (B) thin films deposited onto ultraoriented PTFE substrates at $T_s = 25$ and 90 °C, respectively. The deposition rate was in the range 2.5−3.0 nm/min. The white arrows indicate the PTFE chain axis direction.

of polymorphism in the sublimed thin films as a function of increasing substrate temperature and film thickness.[6,11] Second, we will study how the substrate temperature affects the in-plane orientation of the pentacene domains on the PTFE substrate, and finally, we will establish the in-plane orientation of the ACNs onto oriented PTFE using selected area electron diffraction (SAED).

*(a) Polymorphism as a Function of Substrate Temperature and Film Thickness.* X-ray diffraction (XRD) in ($\theta$, $2\theta$) mode was used to follow the evolution of the crystalline order perpendicular to the substrate plane with increasing $T_s$. Figure 6 depicts the evolution of the XRD spectra of 50 nm PEN films as a function of increasing substrate temperature.

PEN films grown at room temperature exhibit a sequence of diffraction peaks with maxima at 1.57, 0.784, 0.521, and 0.388 nm. These peaks correspond to $(00n)_\alpha$ reflections ($1 \le n \le 4$) of α-PEN and indicate a preferential orientation of the crystalline domains, i.e., a dense $(001)_\alpha$ contact plane on PTFE. Peaks at 1.46 and 0.73 nm correspond to $(00n)_\beta$ reflections ($1 \le n \le 2$) of $\beta$-PEN and indicate the presence of a minority fraction of the $\beta$ phase. For $T_s \ge 50$ °C, the $\beta$ phase becomes dominant. This phase is preferentially oriented with a dense $(001)_\beta$ contact plane on the PTFE surface. Increasing $T_s$ to 90 °C results in (i) the disappearance of α-PEN reflections and (ii) an increase of the intensity of $\beta$-PEN reflections. This $\alpha \rightarrow \beta$ phase transition with increasing $T_s$ has also been reported in the case of silicon and sapphire substrates.[3,5,6]

At $T_s$ = room temperature, we also observe an $\alpha \rightarrow \beta$ transition with increasing film thickness $h$. For $h \le 50$ nm, the most intense reflections correspond to $(00n)_\alpha$ reflections of the α phase. For $h > 50$ nm, the $(00n)_\beta$ reflections of the $\beta$ phase become more intense, indicating a progressive $\alpha \rightarrow \beta$ transition as $h$ increases. This change in crystal structure with film thickness is not observed for $T_s \ge 50$ °C: films grow in the $\beta$ structure from the very beginning of film deposition.

In both these cases, the $\alpha \rightarrow \beta$ transition coincides with a corresponding change in crystal size. A similar phenomenology was observed in the case of phthalocyanines.[25] In phthalocyanines, the relative stability of the α and $\beta$ polymorphs relates to the size of the crystals: small crystals grow in the α structure and large ones in the $\beta$ structure. This size effect is driven by a competition between the surface and bulk energy terms.

The $T_s$-dependence of the crystal structure in TEN films differs in two points from that of PEN, namely, (i) the presence of a single phase in the range $-25$ °C $\le T_s \le 40$ °C and (ii) the lower $T_s$ required to grow oriented films of the triclinic TEN structure. Similarly to PEN, TEN thin films exhibit a preferential orientation on PTFE with a dense (001) contact plane (25 °C $\le T_s \le 40$ °C). The presence of a single phase of TEN in the whole explored $T_s$ range is in agreement with previous reports indicating that the triclinic modification undergoes a structural transformation only for $T$ below $-60$ °C.[26]

*(b) In-Plane Orientation as a Function of Increasing $T_s$.* In Figure 7, we present two sequences of ED patterns obtained for 50-nm-thick TEN and PEN films grown at various $T_s$. Powder-like ED patterns consisting of continuous diffraction rings are observed for TEN and PEN films grown at $T_s$ below $-25$ and 28 °C, respectively, indicating the absence of in-plane orientation. The ED reflections of α-PEN films ($T_s = 27$ °C) correspond to characteristic reticular distances of 0.473, 0.385, 0.298, 0.234, and 0.193 nm. No crystal structure refinement of the α polymorph was proposed so far, given the impossibility to grow large single crystals of this polymorph. However, the ED pattern of α-PEN films grown at room temperature (see Figure 8) exhibits a striking resemblance with that of the TEN film grown at $-27$ °C and there is almost a one-to-one correspondence in the positions of the main diffraction peaks of TEN and α-PEN. This indicates that the structure of α-PEN is likely isomorphous to that of TEN in the (001) plane. Since the triclinic structures of TEN and $\beta$-PEN are identical with respect to the $a$, $b$, and $\gamma$ unit cell parameters, we propose that the α and $\beta$ polymorphs of PEN have very close $a$, $b$, and $\gamma$ unit cell parameters and that the major structural difference lies

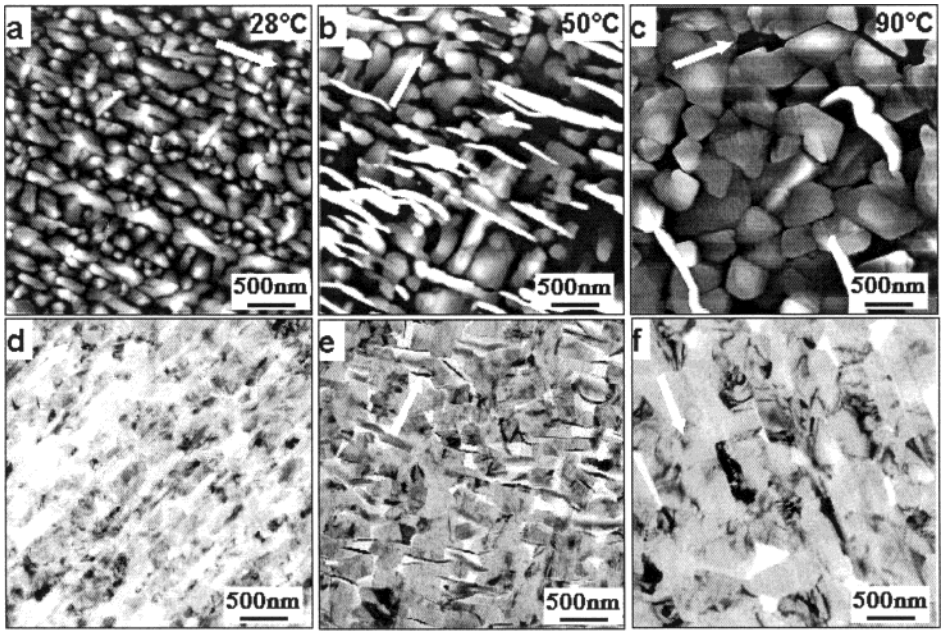


**Figure 4.** Upper and lower sequences: $T_s$-dependence of thin film morphology studied by AFM (a−c) and TEM (d−f), respectively, in PEN/PTFE. Films were grown at a constant deposition rate in the range 2.5−3.0 nm/min. The white arrows indicate the PTFE chain direction i.e., $c_{PTFE}$.

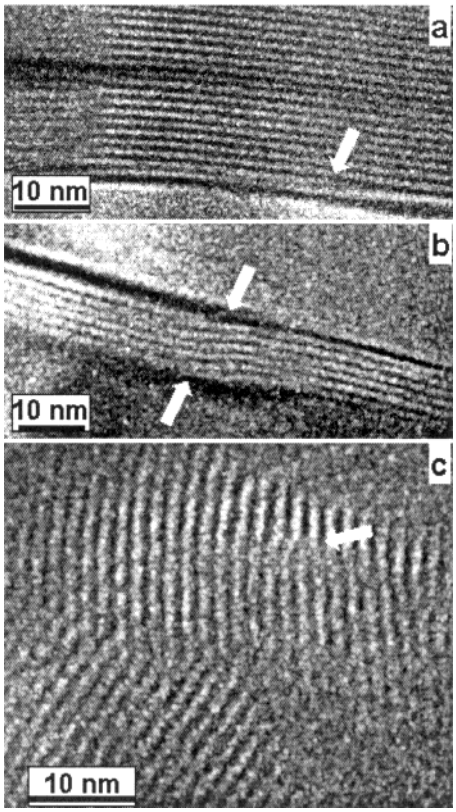


**Figure 5.** Structural defects found in standing edge-on crystallites of PEN ($T_s = 50$ °C, $\tau = 3.0$ nm/min) onto PTFE substrate. Dark stripes correspond to a section of the molecular planes of α-PEN.

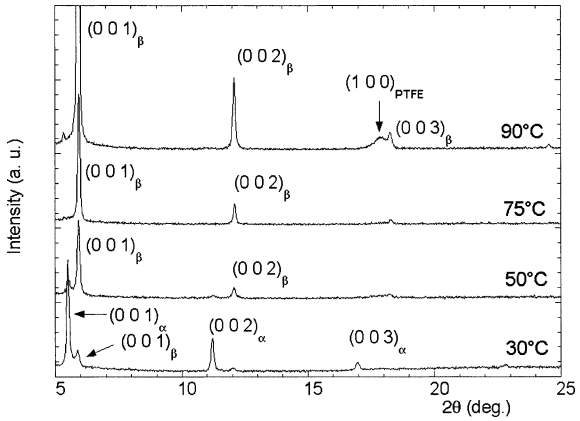


**Figure 6.** Sequence of X-ray diffractograms obtained for 50-nm-thick PEN films grown onto oriented PTFE as a function of increasing $T_s$ (30 °C ≤ $T_s$ ≤ 90 °C; deposition rate $\tau$ between 2.5 nm/min and 3.0 nm/min). For sake of clarity, the diffractograms were shifted along the intensity axis.

in the molecular inclination of the PEN molecules in the (001) plane. Further investigations using SAED are in progress and will be presented in a forthcoming paper.

The nonoriented TEN films ($T_s = -25$ °C) show the typical reflections of the triclinic structure by Campbell et al.[1] (see Table 1): $d_{1\bar{1}0} = 0.466$ nm, $d_{02\bar{1}} = 0.394$ nm, and $d_{12\bar{1}} = 0.322$ nm.

By increasing $T_s$, the powder-like ED pattern of TEN and PEN is progressively replaced by a pattern of sharp reflections. In PEN films, sharp reflections characteristic of oriented domains start to be visible for $T_s = 50$ °C. The best orientation is observed in PEN films grown at $T_s = 90$ °C (re-evaporation is observed for higher $T_s$). The ED pattern for $T_s = 90$ °C shows only sharp reflections with negligible arcing, indicating an excellent in-plane orientation over large PTFE areas (a few millimeters). Accordingly, similarly to other conjugated systems,[18,19] the degree of in-plane orientation on PTFE is found to increase with increasing $T_s$.

*(c) Selected Area Electron Diffraction (SAED).* To index properly the ED pattern of the oriented TEN and PEN films, we performed SAED. Typical SAED patterns of TEN and $\beta$-PEN single domains are shown in Figure 8 together with the corresponding simulated ED patterns. It is worth noticing that the simultaneous presence of the ED patterns of $\beta$-PEN (TEN) and PTFE substrate allows for a precise calibration of the reticular distances using the typical (0 0 15) reflection of PTFE. For the simulations of the ED pattern of PEN, we considered both the reduced unit cell of the $\beta$ form and the $\gamma$ structure.

The triclinic structures of TEN and PEN determined by Campbell et al. gave the best agreement with the experimental SAED patterns and allowed us to reproduce both the intensities

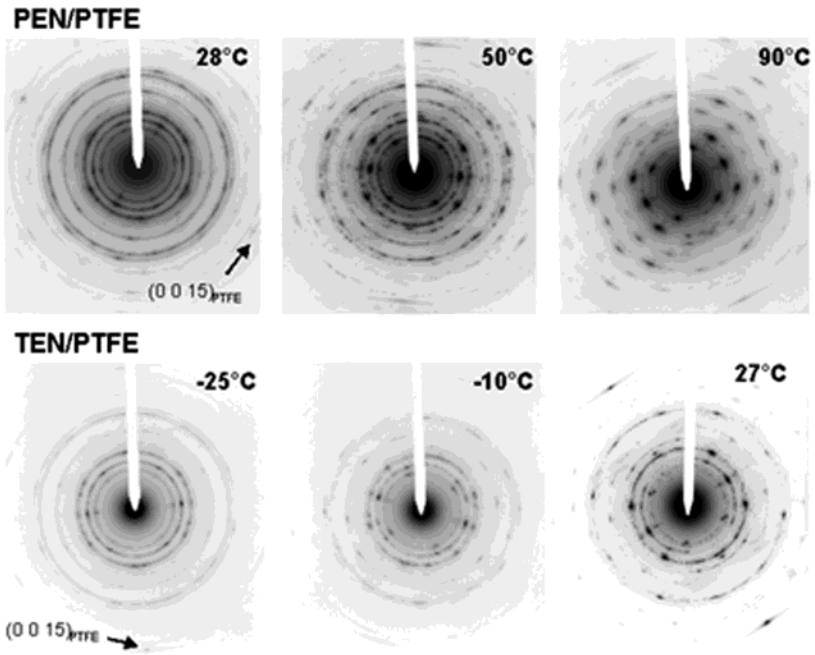


**Figure 7.** Electron diffraction patterns of oriented TEN and PEN films grown onto ultraoriented PTFE substrate at various $T_s$. The deposition rate $\tau$ was in the range 2.5−3.0 nm/min.

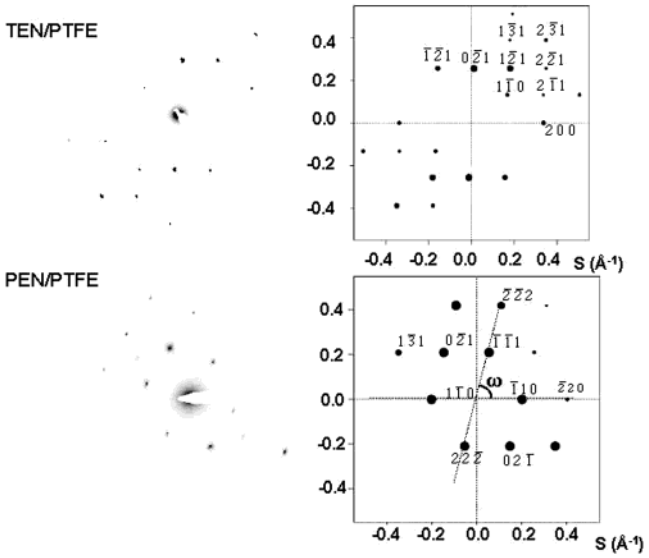


**Figure 8.** SAED and calculated ED pattern for TEN and PEN single crystalline domains in oriented films grown at 25 and 90°C, respectively.

and $d_{hkl}$ values of the reflections. As seen in Figure 8, an excellent agreement between experimental and calculated ED pattern for PEN films is obtained for a [112] zone axis. This orientation of the incident e-beam results in a (001) contact plane, in agreement with the previous results gained from XRD. Not only are the calculated intensities and $d_{hkl}$ values very close to the experimental data but also the angle $\omega$ between ($hh\bar{h}0$) and ($hh\bar{h}$) layer lines (see Figure 8). The calculated value for $\omega$ amounts to 75° for the triclinic $\beta$ structure by Campbell vs 74° for the experimental value. It has to be stressed that the $\gamma$ structure determined recently by various groups yields $\omega$ = 83.5°, which is clearly different from the experimental value and allows us to identify unambiguously the dominant crystal structure in the PEN films for $T_s \geq 50$ °C as the $\beta$ phase. In the case of TEN, a good agreement with the experimental SAED pattern is obtained for a [012] zone axis with a 3° tilt of the film plane with respect to the e-beam direction. In both TEN and PEN films, the [012] and [112] directions are almost parallel to the (001) direction of the incident e-beam and therefore can contribute to the overall ED pattern. The orientation of the (02$\bar{1}$) reflection of PEN (TEN) relative to the PTFE (0 0 15) reflection indicates that the *a* axis of the ACN overlayer is parallel to the PTFE chain axis direction $c_{PTFE}$. The overlayer−substrate crystallographic relationship obtained from ED and XRD can accordingly be summarized as follows: $(001)_{ACN}||(010)_{PTFE}$ and $[100]_{ACN}||[001]_{PTFE}$.

**III.3. Optical Properties.** The evolution of the optical absorption spectrum of PEN films deposited onto PTFE at various $T_s$ reflects the structural and morphological modifications probed by TEM and AFM. Figure 9 depicts the anisotropy of the absorption spectrum of crystalline α-PEN ($T_s$ = 28 °C) and $\beta$-PEN ($T_s$ = 90 °C) thin films. All the absorption spectra exhibit the typical vibronic structure with the 0−0, 0−1, and 0−2 transitions as observed by Zanker and Preuss for $\beta$-PEN single crystals.[27] In addition, we also observe the splitting of the 0−0 transition ($^1$L transition) in two $^1L_a$ and $^1L_b$ transitions that are polarized along *a* and *b* crystallographic directions of $\beta$-PEN, respectively.[27] These two components are separated by the Davydov exciton splitting Δ, which is a direct measure of the resonance interaction energy between two nonequivalent PEN molecules in the unit cell.[28] As seen from Table 2, the position of the low-energy component $^1L_a$ is almost unaffected by the structural/morphological modifications. The maximum absorption is located at 14 973 ± 20 cm$^{-1}$ in α-PEN and around 14 960 ± 20 cm$^{-1}$ in $\beta$-PEN. In contrast to this, the position of the $^1L_b$ component shows a sizable shift with increasing $T_s$. It is centered at 15 870 ± 20 cm$^{-1}$ in α-PEN ($T_s$ = 25 °C) and 15 960 ± 20 cm$^{-1}$ in $\beta$-PEN films ($T_s$ = 90 °C). Accordingly, the Davydov splitting for α and $\beta$ polymorphs in thin films deposited onto PTFE are 897 ± 40 cm$^{-1}$ and 990 ± 40 cm$^{-1}$. Both of these values of Δ are below the 1100 cm$^{-1}$ reported for $\beta$-PEN single crystals.[27] Bässler and co-workers observed that the Davydov splitting in quasiamorphous PEN films deposited at $T_s$ = 80 K is significantly smaller than that of $\beta$-PEN single crystals, typically 880 ± 70 cm$^{-1}$.[29] The $T_s$-dependence of Δ can be

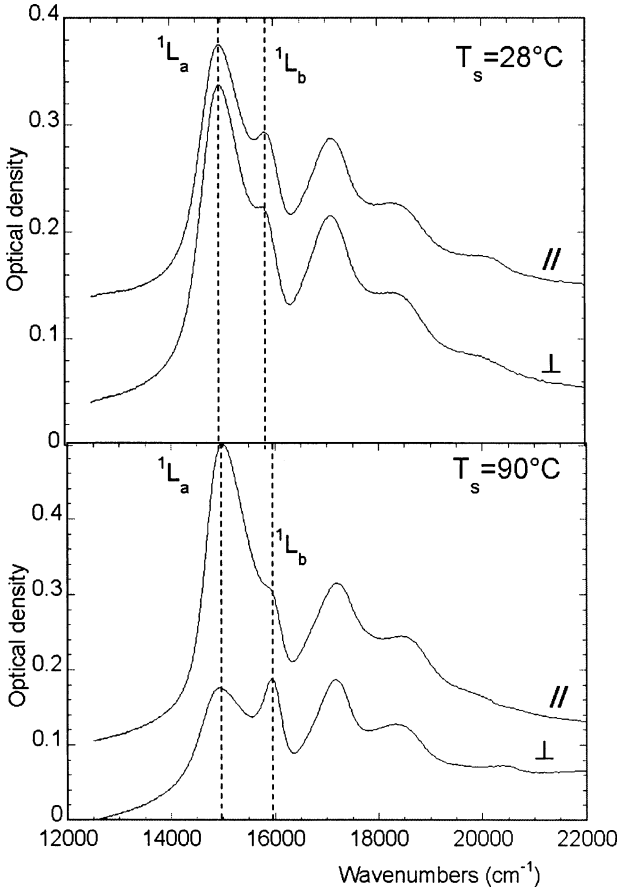


**Figure 9.** In-plane anisotropy of the absorption spectrum of PEN thin films onto oriented PTFE for $T_s = 28$ and 90 °C. The spectra were shifted along the ordinate axis to clarify the whole figure.

**TABLE 2: Dependence of Dichroic Ratio, $^1L_a$ and $^1L_b$ Band Positions, and Davydov Splitting upon Substrate Temperature for 50 nm Films Deposited onto PTFE[a]**

| sample, $T_s$ (°C) | dr($^1L_a$) = $OD_{\parallel}/OD_{\perp}$ | $^1L_b$ (cm$^{-1}$) | $^1L_a$ (cm$^{-1}$) | $\Delta$ (cm$^{-1}$) |
|---|---|---|---|---|
| 30 | 1.1 | 14973 | 15870 | 920 |
| 50 | 1.4 | 14976 | 15912 | 936 |
| 70 | 2.0 | 14940 | 15937 | 997 |
| 90 | 2.5−3.0 | 14970 | 15960 | 990 |

[a] Spectral positions of the $^1L_a$ and $^1L_b$ components were determined by fitting the spectra with five Gaussian components.

attributed to the conjunction of several factors, e.g. (i) the change of crystal structure $\alpha \rightarrow \beta$, (ii) size effects as in cyanine aggregates,[30] and (iii) different concentrations of structural defects, as evidenced by HRTEM. The lower value of $\Delta$ found in crystalline $\beta$-PEN films grown at $T_s = 90$ °C with respect to single-crystals may be attributed to a higher concentration of structural defects or a different crystal structure. In addition, the observation of Davydov splitting in α-PEN films indicates the presence of dimers of PEN as in $\beta$-PEN but in a slightly different arrangement.

As seen in Figure 9, the in-plane orientation of $\beta$-PEN results in a significant anisotropy of the $^1L_a$ band. In agreement with previous results on single-crystals, the maximum absorbance of the $^1L_a$ band is observed for incident light polarized parallel to $c_{PTFE}$ i.e., to $a_{ACN}$. The $^1L_b$ band is polarized in a direction perpendicular to $c_{PTFE}$ but with a smaller dichroic ratio than the $^1L_a$ band. For instance, at $T_s = 90$ °C, dr($^1L_a$) = 2.5−3.0, whereas dr($^1L_b$) = 1.6. This is attributed to the fact that $b_{PEN}$ is not strictly perpendicular to $c_{PTFE}$.

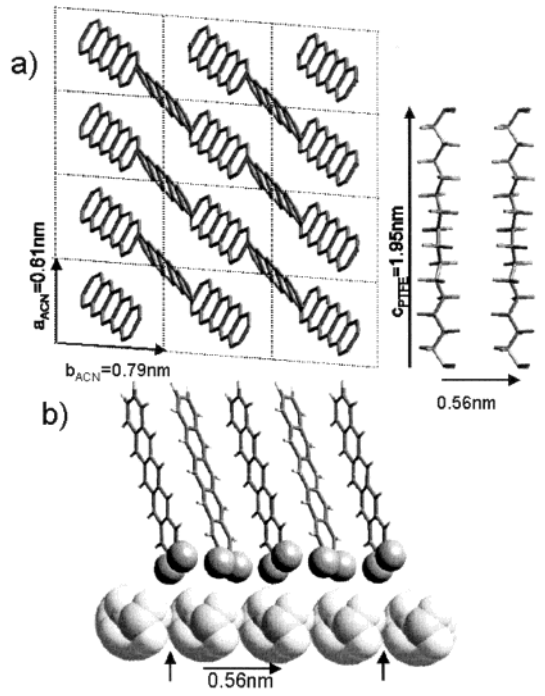


**Figure 10.** Overlayer and substrate unit cells at the PEN/PTFE interface: (a) top-view and (b) section of the PEN/PTFE interface.

The dichroic ratio of the $^1L_a$ band is clearly increasing with increasing $T_s$ between 1.1 for $T_s = 28$ °C and 2.5−3.0 for $T_s = 90$ °C (see Table 2). The dichroic ratio obtained in our case is identical to that reported by Chen et al. for oriented PEN deposited onto an ultrathin PEN layer oriented by rubbing[12] and by Swiggers et al., who used oriented poly(vinyl alcohol) substrates.[13]

## IV. Discussion

In this section, we will analyze our experimental observations successively in terms of classical epitaxy (1D and 2D) and ledge-directed nucleation followed by confined growth.

**(a) Structure of the ACN/PTFE Interface.** The contact plane of PEN and its orientation with respect to the PTFE chains is depicted in Figure 10. The dense (001) contact plane of TEN and PEN is characterized by the following unit cell parameters: $a = 0.60$ nm, $b = 0.79$ nm, and $\gamma = 93.7°$ for TEN and $a = 0.606$ nm, $b = 0.79$ nm, and $\gamma = 94.2°$ for PEN. Within the $(001)_{PEN}$ plane, the long axis of the PEN molecules is tilted 15° from the normal to the contact plane (see Figure 10). ACN molecules are arranged into dimers close-packed along the $a$ direction at a repeat distance of 0.61 nm. The "standing" orientation of ACN molecules traduces the poor affinity of the apolar and fully conjugated ACN molecules for the polar $CF_2$ units forming the PTFE chains. This molecular orientation of ACNs on PTFE maximizes intermolecular interactions between ACN molecules, $E_{MOL-MOL}$ (which include both dispersive van der Waals and $\pi-\pi$ contributions), and minimizes interactions with the substrate, $E_{MOL-PTFE}$.[31]

**(b) Analysis in Terms of 1D- and 2D-Epitaxy.** To establish epitaxial relations at the ACN/PTFE interface, we used the high-temperature phase of PTFE ($T > 19$ °C), which is described by a pseudohexagonal unit cell with $a = b = 0.566$ nm, $c = 1.95$ nm and $\alpha = \beta = 90°$, $\gamma = 120°$, since oriented films of TEN and PEN are observed only for $T_s > 25$ °C. The PTFE surface of the films is a crystallographic ($a$, $c$) plane. However, due to numerous structural defects, e.g. helix reversal defects, the PTFE

surface should rather be regarded as a disordered plastic crystalline phase, especially for $T > 50$ °C.[32]

First, the periodicity between adjacent stacks of ACNs ($a/2 = 0.395$ nm) is different from the interchain periodicity of PTFE (0.56 nm). The simplest 1D epitaxial relation found in the direction perpendicular to the PTFE chains is $2b_{ACN} = 3a_{PTFE}$. In this situation, only one row of ACN molecules over four lies in a favorable position on the substrate (likely a groove between successive PTFE chains), as depicted in Figure 10. We therefore consider that 1D epitaxy in the direction perpendicular to $c_{PTFE}$ cannot explain the orientation of ACNs onto oriented PTFE.

In the direction parallel to $c_{PTFE}$, a matching condition of the type $3a_{ACN} = c_{PTFE}$ (6% mismatch) can be found. However, given the numerous helicity defects for $T > 50$ °C,[32] we consider that 1D-epitaxy along $c_{PTFE}$ cannot be regarded as the driving force for the orientation of ACNs.

Considering 2D-epitaxy, it can hardly be supported given the large $3a_{ACN}*2b_{ACN}$ supercell (surface of 2.9 nm$^2$) and the small fraction (25%) of "stabilized" ACN molecules on the PTFE surface. The major argument against 2D-epitaxy is the absence of PEN and TEN monolayers onto flat PTFE areas in the early stage of growth.

**(c) Ledge-Directed Nucleation and Confined Growth.** Our observations clearly underline the prime role of PTFE ledges in both nucleation and confinement of crystal growth. In classical models of heterogeneous nucleation at a ledge, one can write the free energy of nucleation of a faceted crystal as[21]

$$\Delta G_{nucl} = \sum_{hkl} A_{hkl}\gamma_{hkl} - A_{cs}\gamma_{cs} - \Delta G_c \qquad (1)$$

where $A_{hkl}$ and $\gamma_{hkl}$ are the areas and the surface free energies of the *hkl* facets. $\Delta G_c$ is the free energy associated with the phase change (gas to solid) and cs index refers to the crystal/surface interface.

If the aggregate morphology matches the topography of the ledge, there is a significant reduction of $\Delta G_{nucl}$, since $\sum_{hkl}A_{hkl}\gamma_{hkl}$ is lowered at the expense of the interfacial contribution $A_{cs}\gamma_{cs}$. In the case of TiOPc,[19] preferential nucleation at PTFE ledges was qualitatively explained by noticing that the PTFE ledge structure matches that of the TiOPc crystal at the contact interface. It was proposed that PTFE macrosteps are formed by the intersection between two crystallographically equivalent planes $(100)_{PTFE} \cap (010)_{PTFE}$ as depicted in Figure 11. Under this assumption and using the orientations of the TEN and $\beta$-PEN crystals on PTFE as determined from ED, it turns out that the dense $(01\bar{1})_{ACN}$ facets are almost parallel to the $(100)_{PTFE}$ plane of the PTFE ledge. In fact, $(100)_{PTFE} \cap (0\bar{1}0)_{PTFE} = 120°$ whereas $(01\bar{1})_{PEN} \cap (001)_{PEN} = 112.6°$ and $(01\bar{1})_{TEN} \cap (001)_{TEN} = 113.2°$, leading to angular mismatches of 7.4° and 6.8°, respectively.

With respect to earlier reports on ledge-directed nucleation, these angular mismatches appear rather large. In the case of benzoic acid (BA) grown onto succinic acid (SA), a mismatch of 0.6° is found between $(100)_{BA} \cap (112)_{BA}$ and $(0\bar{1}0)_{SA} \cap (1\bar{1}1)_{SA}$.[31,33] In the absence of strong ACN−PTFE interactions, we propose that the dihedral angular mismatch at the PTFE ledge can be overcome by a slight deformation of the molecular orientation in the first ACN layer in contact with the PTFE surface.

Beside nucleation, our results show that PTFE nanofibrils play a key role in the dynamics of crystal growth. Our observations indicate that PTFE nanofibrils are responsible for anisotropic mass transport along the chain axis of PTFE,

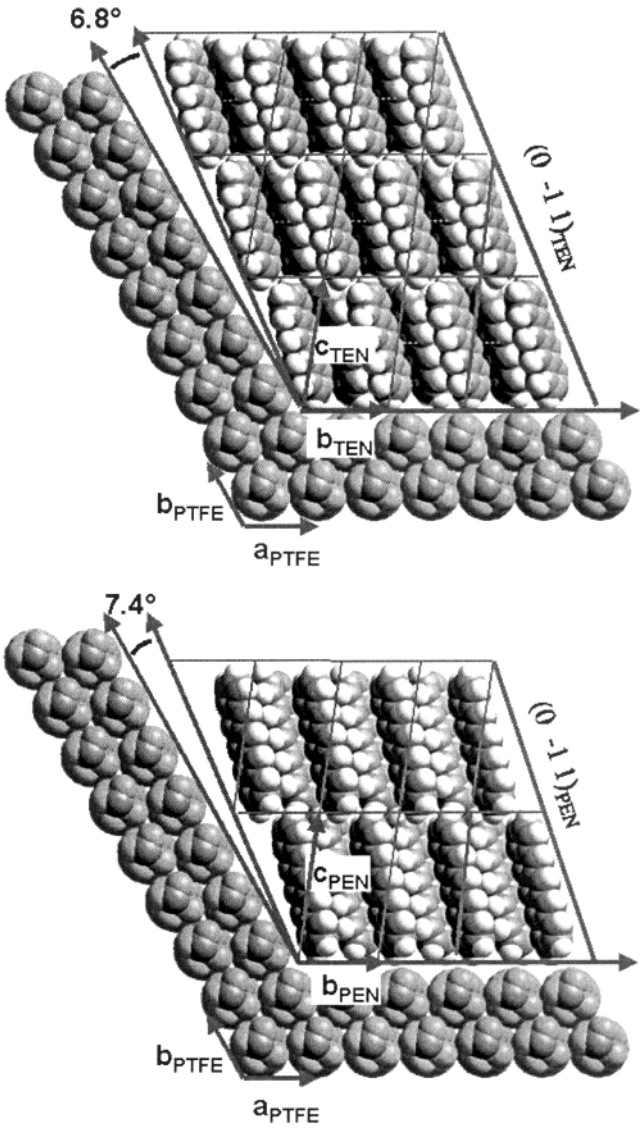


**Figure 11.** Molecular model of oriented nuclei of TEN (top) and PEN (bottom) at PTFE ledge sites illustrating the dihedral angle match (see text). The PTFE ledge structure is represented by the intersection $(100)_{PTFE} \cap (010)_{PTFE}$.

hindering the lateral growth of pentacene crystallites perpendicular to $c_{PTFE}$ in the early stage of growth (see Figure 2). The anisotropy of mass transport on the oriented PTFE surface is related to both the nanoscale relief of the substrate and the intrinsic anisotropy of molecular diffusion on oriented PTFE. This preferential mass transport along $c_{PTFE}$ will enhance crystal growth in the direction parallel to the PTFE fibrils. Since molecular diffusion on the surface and molecular reorganizations in the grains are both thermally activated processes, we can understand that the orientation mechanism is improved by increasing $T_s$. Finally, oriented growth of ACNs onto oriented PTFE can be understood as the conjunction of both (i) topographically directed nucleation at PTFE ledges and (ii) confined crystal growth by the PTFE meso- and nanoscale relief.

These results raise the question of how to master the spatial distribution and size of the PTFE ledges in order to control the morphology and crystal size of the deposited material. So far, we have not succeeded in controlling all aspects of PTFE deposition. This is due to the fact that the parameters governing the friction-transfer of PTFE are numerous, e.g. the pressure of the PTFE rod on the glass substrate, the roughness of both the PTFE rod and substrate surfaces, the temperature of substrate

before and during friction, and the speed of friction. A simple way to control the density of PTFE ledges would be to use a micropatterned PTFE rod. Experiments in this direction are currently in progress.

## V. Conclusions

We have demonstrated the possibility to grow oriented films of TEN and $\beta$-PEN onto oriented PTFE substrate. Films of TEN and PEN exhibit the same in-plane orientation, namely, $a_{ACN}||c_{PTFE}$, and a dense (001) contact plane. ACN molecules are almost in a standing position and form dimers that are closely packed along $a_{ACN}$. The best orientation in TEN and PEN thin films is achieved for $T_s \geq 25$ °C and $T_s \geq 70$ °C, respectively. PEN thin films grow essentially in the α form for $T_s < 50$ °C and in the $\beta$ form for $T_s \geq 50$ °C. The prime role of PTFE ledges and grooves between PTFE nanofibrils in the heterogeneous nucleation and orientation of growth has been evidenced. No evidence for epitaxy is observed in the case of pentacene and tetracene. However, the analysis of the early stage of oriented growth suggests that orientation of TEN and PEN is mainly due to the conjunction of (i) topographically directed nucleation at PTFE ledges and (ii) confined and directional growth of nanocrystals by the PTFE mesorelief. This orientation mechanism is believed to occur because of the poor affinity between the PTFE chains and the conjugated ACN molecules contrarywise to alkyl-substituted molecules. More generally, our results illustrate the possibility to control oriented nucleation via the ledges of a nanostructured and oriented polymer surface. Tailoring the density and the size of the ledges will undoubtedly provide better control over the oriented film morphology.

**Acknowledgment.** We acknowledge support by EEC contract HPRN-CT-2002-0327 and the Swiss National Science Foundation under contract 20-67929.02. Fruitfull discussions with Annette Thierry, Marc Schmutz and Bernard Lotz are gratefully acknowledged. Michel Longchamp is also acknowledged for technical support.

## References and Notes

(1) (a) Campbell, D. J.; Robertson, J. M.; Trotter, J. *Acta Crystallogr.* **1961**, 14, 705; (b) *Acta Crystallogr.* **1962**, *15*, 289.

(2) (a) Friend, R. H.; Gymer, R. W.; Holmes, A. B.; Burroughes, J. H.; Marks, R. N.; Taliani, C.; Dos Santos, D. A.; Brédas, J.-L.; Lögdlund, M.; Salaneck, W. R. *Nature* **1999**, *397*, 121. (b) Dimitrakopoulos, C. D.; Malenfant, R. L. *Adv. Mater.* **2002**, *14*, 99.

(3) Dimitrakopoulos, C. D.; Brown, A. R.; Pomp, A. *J. Appl. Phys.* **1996**, *80*, 2501.

(4) Laquindanum, J. G.; Katz, H. E.; Lovinger, A. J.; Dodabalapur, A. *Chem. Mater.* **1996**, *8*, 2542.

(5) (a) Lin, Y. Y.; Gundlach, D. J.; Nelson, S. F.; Jackson, T. N.; *IEEE Trans. Elect. Dev.* **1997**, *44*, 1325. (b) Gundlach, D. J.; Nichols, J. A.; Zhou, L.; Jackson, T. N. *Appl. Phys. Lett.* **2002**, *80*, 2925.

(6) (a) Knipp, D.; R. A. Street and Ho, J. *J. Appl. Phys.* **2003**, *93*, 347. (b) Jentzsch, T.; Juepner, H. J.; Brzezinka, K.-W.; Lau, A. *Thin Solid Films* **1998**, *315*, 273.

(7) Meyer zu Heringdorf, F. J.; Reuter, M. C.; Tromp, R. M. *Nature* **2001**, *412*, 517.

(8) Brown, A. R.; Pomp, A. J.; de Leeuw, D. M.; Klaassen, D. B. M.; Havinga, E. E.; Herwig, P.; Müllen, K. A. *Appl. Phys.* **1996**, *79*, 2136.

(9) Mattheus, C. C.; Dros, A. B.; Baas, J.; Meetsma, A.; de Boer, J. L.; Palstra, T. T. M. *Acta Crystallogr. C* **2001**, *57*, 939.

(10) Holmes, D.; Kumaraswamy, S.; Matzger, A. J.; Vollhardt, P. C. *Chem. Eur. J.* **1999**, *5*, 3399.

(11) Bouchoms, I. P. M.; Schoonveld, W. A.; Vrijmoeth, J.; Klapwijk, T. M. *Synth. Met.* **1999**, *104*, 175.

(12) Chen, X. L.; Lovinger, A. J.; Bao, Z. N.; Sapjeta, *J. Chem. Mater.* **2001**, *13*, 1341.

(13) Swiggers, M. L.; Xia, G.; Gorodetsky, A. A., Malliaras, G. G.; Headrick, R. L.; Weslowski, B. T.; Shashidhar, R. N.; Dulcey, C. S. *Appl. Phys. Lett.* **2001**, *79*, 1300.

(14) Wittmann, J.-C.; Smith, P. *Nature* **1991**, *352*, 414.

(15) Lang, P.; Horowitz, G.; Valat, P.; Garnier, F.; Wittmann, J.-C.; Lotz, B. *Phys. Chem. B* **1997**, *101*, 8204.

(16) Gill, R. E.; Hadziioannou, G.; Lang, P.; Garnier, F.; Wittmann, J.-C. *Adv. Mater.* **1997**, *9*, 331.

(17) (a) Ueda, H.; Kuriyama, T.; Hari, T.; Watanabe, M.; Ni, J.; Hattori, Y.; Ueniski, N.; Uemiya, T. *Jpn. J. Appl. Phys.* **1995**, *34*, 3876. (b) Lemoigne, J.; Kajzar, A.; Thierry, A. *Macromolecules* **1991**, *24*, 2622.

(18) Moulin, J.-F.; Brinkmann, M.; Thierry, A.; Wittmann, J.-C. *Adv. Mater.* **2002**, *14*, 436.

(19) (a) Manaka, T. Tagushi, K.; Ishikawa, K.; Takezoe, H. *Jpn. J. Appl. Phys.* **2000**, 39, 4910. (b) Brinkmann, M.; Wittmann, J. C.; Barthel, M.; Hanack, M.; Chaumont, C. *Chem. Mater.* **2002**, *14*, 904.

(20) (a) Tanaka, T.; Ishitobi M. *J. Phys. Chem. B* **2002**, *106*, 564. (b) Tanaka, T.; Honda, Y.; Ishitobi, M. *Langmuir* **2001**, *17*, 2192. (c) Tanaka, T.; Matsuoka, M. *Thin Solid Films* **2001**, *393*, 148.

(21) (a) Yan, S.; Katzenberg, F.; Petermann, J.; Yang, D.; Shen, Y.; Straupé, C.; Wittmann, J.-C.; Lotz, B. *Polymer* **2000**, *41*, 2613. (b) Damman, P.; Dosière, M., Brunel, M.; Wittmann, J.-C. *J. Am. Chem. Soc.* **1997**, *119*, 4633. (c) Vallée, R.; Dosière, M., Toussaere, E.; Zyss. J. *J. Am. Chem. Soc.* **2000**, *122*, 6701.

(22) M. Carrara, Thesis, Ecole Polytechnique Fédérale de Lausanne, 2002.

(23) Drummy, L. F.; Kübel, C.; Lee, D.; White, A.; Martin, D. C. *Adv. Mater.* **2002**, *14*, 54.

(24) Eberhardt, J.-P. In *Analyse structurale et chimique des matériaux*; France, 1989; pp 460−465.

(25) (a)Yim, S.; Heutz, S.; Jones, T. S. *J. Appl. Phys.* **2002**, *91*, 3632. (b) Iwatsu, F. *J. Phys. Chem.* **1988**, *92*, 1678.

(26) Sondermann, U.; Kutoglu, A.; Bässler, H. *J. Phys. Chem.* **1985**, *89*, 1735.

(27) Zanker, V.; Preuss, J. *Z. Angew. Phys.* **1969**, *27*, 363.

(28) Pope, M. In *Electronic processes in organic crystals*; Oxford University Press: Oxford, 1982; p 26.

(29) Hesse, R.; Hofberger, W.; Bässler, H. *Chem. Phys.* **1980**, *49*, 201.

(30) Nüesch, F.; Grätzel, M. *Chem. Phys.* **1995**, *193*, 1.

(31) Ward, M. D. *Chem. Rev.* **2001**, *101*, 1697.

(32) Kimmig, M.; Strobl, G.; Stühn, B. *Macromolecules* **1994**, *27*, 2481.

(33) Carter, P. W.; Ward, M. D. *J. Am. Chem. Soc.* **1993**, *115*, 11521.